The Astrophysical Journal, 725:1587–1599, 2010 December 20 doi:10.1088/0004-637X/725/2/1587
© 2010. The American Astronomical Society. All rights reserved. Printed in the U.S.A.

$z \sim 7$ GALAXY CANDIDATES FROM NICMOS OBSERVATIONS OVER THE HDF-SOUTH AND THE CDF-SOUTH AND HDF-NORTH GOODS FIELDS*

Rychard J. Bouwens[1,2], Garth D. Illingworth[1], Valentino González[1], Ivo Labbé[3,9], Marijn Franx[2], Christopher J. Conselice[4], John Blakeslee[5], Pieter van Dokkum[6], Brad Holden[1], Dan Magee[1], Danilo Marchesini[7], and Wei Zheng[8]

[1] Astronomy Department, University of California, Santa Cruz, CA 95064, USA
[2] Leiden Observatory, Leiden University, Postbus 9513, 2300 RA Leiden, The Netherlands
[3] Carnegie Observatories, Pasadena, CA 91101, USA
[4] School of Physics and Astronomy, University of c Nottingham, Nottingham, NG72RD, UK
[5] Herzberg Institute of Astrophysics, Victoria, BCV9E2E7, Canada
[6] Department of Astronomy, Yale University, New Haven, CT 06520, USA
[7] Department of Physics and Astronomy, Tufts University, Medford, MA 02155, USA
[8] Department of Physics and Astronomy, Johns Hopkins University, 3400 North Charles Street, Baltimore, MD 21218, USA
Received 2010 March 9; accepted 2010 October 13; published 2010 November 30

ABSTRACT

We use ∼88 arcmin^2 of deep ($\gtrsim$26.5 mag at 5σ) NICMOS data over the two GOODS fields and the HDF-South to conduct a search for bright $z \gtrsim 7$ galaxy candidates. This search takes advantage of an efficient preselection over 58 arcmin^2 of NICMOS H_{160}-band data where only plausible $z \gtrsim 7$ candidates are followed up with NICMOS J_{110}-band observations. ∼248 arcmin^2 of deep ground-based near-infrared data ($\gtrsim$25.5 mag, 5σ) are also considered in the search. In total, we report 15 z_{850}-dropout candidates over this area—7 of which are new to these search fields. Two possible $z \sim 9$ J_{110}-dropout candidates are also found, but seem unlikely to correspond to $z \sim 9$ galaxies (given the estimated contamination levels). The present $z \sim 9$ search is used to set upper limits on the prevalence of such sources. Rigorous testing is undertaken to establish the level of contamination of our selections by photometric scatter, low-mass stars, supernovae, and spurious sources. The estimated contamination rate of our $z \sim 7$ selection is ∼24%. Through careful simulations, the effective volume available to our $z \gtrsim 7$ selections is estimated and used to establish constraints on the volume density of luminous ($L^*_{z=3}$, or ∼−21 mag) galaxies from these searches. We find that the volume density of luminous star-forming galaxies at $z \sim 7$ is 13^{+8}_{-5} times lower than at $z \sim 4$ and >25 times lower (1σ) at $z \sim 9$ than at $z \sim 4$. This is the most stringent constraint yet available on the volume density of $\gtrsim L^*_{z=3}$ galaxies at $z \sim 9$. The present wide-area, multi-field search limits cosmic variance to $\lesssim$20%. The evolution we find at the bright end of the UV LF is similar to that found from recent Subaru Suprime-Cam, HAWK-I or ERS WFC3/IR searches. The present paper also includes a complete summary of our final $z \sim 7$ z_{850}-dropout sample (18 candidates) identified from all NICMOS observations to date (over the two GOODS fields, the HUDF, galaxy clusters).

Key words: galaxies: evolution – galaxies: high-redshift

Online-only material: color figures

1. INTRODUCTION

The recent WFC3/IR camera on the *Hubble Space Telescope* (*HST*; Kimble et al. 2006) has completely revolutionized our ability to search for galaxies at $z \gtrsim 7$ due to its extraordinary imaging capabilities in the near-infrared—allowing for large areas to be surveyed to great depths. Already some 40 credible $z \sim 7$–8 galaxy candidates have been identified in the first 100 orbits of observations (Oesch et al. 2010a; Bouwens et al. 2010a, 2010b; McLure et al. 2010; Bunker et al. 2010; Yan et al. 2010; Finkelstein et al. 2010; Wilkins et al. 2010a, 2010b). This compares with ∼15 credible candidates reported thus far from deep, wide-area ground-based observations (Ouchi et al. 2009; Castellano et al. 2010; Hickey et al. 2010) and ∼12 thus far with NICMOS (e.g., Bouwens et al. 2008, Bouwens et al. 2009a; Bradley et al. 2008; Oesch et al. 2009; Zheng et al. 2009; ∼2 from Richard et al. 2008). Whereas ∼100 orbits of NICMOS observations were required to find one $z \sim 7$ credible galaxy candidate (see, e.g., Section 4 of Bouwens et al. 2009a), only ∼2.5 orbits of WFC3/IR observations are required to find a similar $z \sim 7$ candidate.

Despite these significant advances in our observational capabilities with WFC3/IR to reach deep and identify large numbers of faint $z \gtrsim 7$ galaxies, a full characterization of the galaxy population at $z \sim 7$ requires that we identify large numbers of galaxies at *both* high and low luminosities. All but ∼6 galaxies in early selections of $z \sim 7$–8 galaxies from early WFC3/IR observations over the ERS/HUDF09 fields have magnitudes faintward of 26.5 mag (e.g., Oesch et al. 2010a; Wilkins et al. 2010a; Bouwens et al. 2010c). As such, it is somewhat challenging to characterize the properties of relatively luminous galaxies at $z \gtrsim 6.5$, and some expansion of the number of sources known brightward of 26.5 mag would be beneficial. Such samples are particularly valuable over fields such as GOODS (Giavalisco et al. 2004) where other valuable multiwavelength data exist like deep IRAC (Dickinson & GOODS Team 2004) or *Chandra* coverage (Brandt et al. 2001; Rosati et al. 2002).

Fortunately, for the selection of luminous $z \sim 7$–8 galaxies, some ∼88 arcmin^2 of deep (>26.5 mag, 5σ), wide-area

* Based on observations made with the NASA/ESA *Hubble Space Telescope*, which is operated by the Association of Universities for Research in Astronomy, Inc., under NASA contract NAS 5-26555. These observations are associated with programs #7235, 7817, 9425, 9575, 9723, 9797, 9803, 9978, 9979, 10189, 10339, 10340, 10403, 10530, 10632, 10872, 11082, 11144, and 11192. Observations have been carried out using the Very Large Telescope at the ESO Paranal Observatory under Program ID(s): LP168.A-0485.
[9] Hubble Fellow.

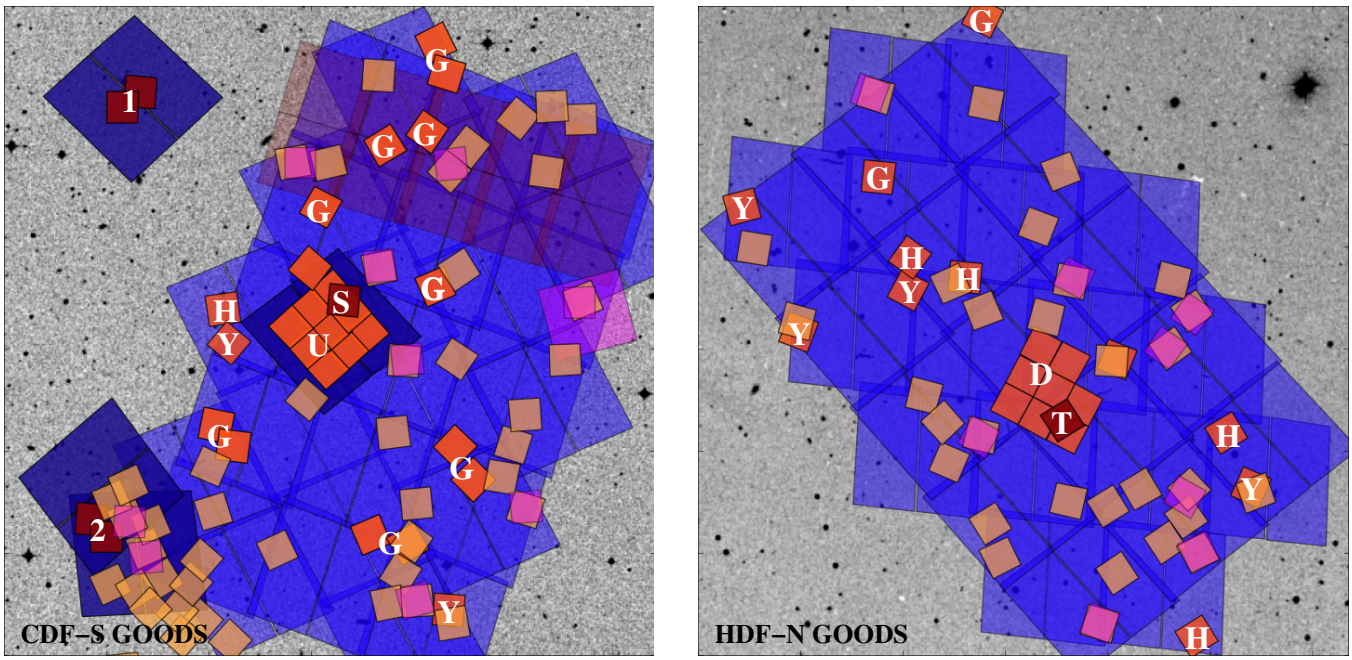

Figure 1. Deep, wide-area near-IR data available to search for $z \gtrsim 7$ galaxies over the CDF-S GOODS (left) and HDF-N GOODS (right) fields (see also Table 1). Most of the ultra-deep NICMOS and deep NICMOS observations were already presented in Bouwens et al. (2008) and are included here (red and dark orange regions corresponding to regions with 5σ depths of $\gtrsim$28 mag and $\gtrsim$26.5 mag, respectively). What is new in the current analysis is the moderately deep (26.9 mag at 5σ), wide-area ($\sim$58 arcmin^2: $>$60 NIC3 pointings) NICMOS H_{160}-band data (light orange squares: Conselice et al. 2010). These data can be used to search for $z \gtrsim 7$ galaxy candidates by identifying those sources that are not detected in the ACS optical bands, have very red $z_{850} - H_{160}$ colors, and possess reasonably blue $H - 5.8\,\mu$m and $3.6\,\mu$m $- 5.8\,\mu$m colors. Unfortunately, these criteria (while very demanding) are not sufficient to place strong enough constraints on the redshift of the candidates, and so we also obtained deep (27.0 mag at 5σ) NICMOS J_{110}-band imaging (magenta squares) over the best $z \gtrsim 7$ candidates (Table 2: see Section 3.2) with GO program 11144 (PI: Bouwens). Also shown in dark orange—and annotated with "Y" or "H" (for the GO11192 H. Yan et al. 2010, in preparation or Henry et al. 2009 fields, respectively)—are several additional NICMOS search fields we used to search for $z \gtrsim 7$ galaxies not considered by Bouwens et al. (2008). NICMOS search fields previously considered by Bouwens et al. (2008) in searches for $z \gtrsim 7$ galaxies are indicated as follows: "D" denotes the HDF-N Dickinson field (Dickinson 1998), "T" denotes the HDF-N Thompson field (Thompson et al. 1999), "U" denotes the HUDF Thompson field (Thompson et al. 2005), "S" denotes the HUDF05 NICMOS field over the HUDF (Oesch et al. 2009), "1" denotes the first set of NICMOS parallels to the HUDF (NICP12: Oesch et al. 2009), "2" denotes the second set of NICMOS parallels to the HUDF (NICP34: Oesch et al. 2009), and "G" denotes the GOODS Parallel NICMOS fields. The blue and dark blue regions correspond to regions with deep and very deep optical ACS coverage, respectively (5σ depths of $\gtrsim$28 and $\gtrsim$29 mag). The position of the ground-based ISAAC+MOIRCS search areas is not shown here to minimize confusion (but is presented in Figure 1 of Bouwens et al. 2008). Also not included on this figure are the NICMOS search fields (Zirm et al. 2007) over the HDF-S (Williams et al. 2000). The position of the Early Release Science WFC3/IR observations with the CDF-S (not used here for $z \sim 7$ LF constraints) is indicated by the light-shaded red region. A link to our NICMOS reductions over the GOODS fields is provided at http://firstgalaxies.org//astronomers-area.

(A color version of this figure is available in the online journal.)

NICMOS observations exist over the two GOODS fields and the HDF-South (HDF-S). While $\sim$23 arcmin^2 of those observations have already been used to identify $z \sim 7$–8 galaxies (Bouwens et al. 2008; Oesch et al. 2009), $\gtrsim$60 arcmin^2 of those data have yet to be used. Most of these data are associated with the GOODS NICMOS survey (Conselice et al. 2010) or are NICMOS parallels associated with other *HST* programs. In total, these NICMOS observations cover twice as much area as available in the WFC3/IR observations that made up the Early Release Science Program (PI: O'Connell; GO 11359). Meanwhile, these observations cover comparable area to that available in the wide-area HAWK-I *Y*-band observations over the CDF-South (CDF-S; Castellano et al. 2010; Hickey et al. 2010) and less area than the Subaru Suprime-Cam (Ouchi et al. 2009) observations over the HDF-North (HDF-N), but are deeper on average (by $\sim$0.2 and $\sim$0.7 mag, respectively).

In the present work, we use these wide-area NICMOS observations to identify a small sample of luminous star-forming galaxies at $z \sim 7$, adding significantly to those known, and performing a search at $z \sim 9$. Some of the present $z \sim 7$ samples have already been used by González et al. (2010) and Labbé et al. (2010b) to perform stellar population modeling of luminous $z \sim 7$ galaxies and to extend measures of the stellar mass density and specific star formation rate to $z \sim 7$. Here we describe the selection of those $z \gtrsim 7$ candidates in detail, discuss the properties and layout of the NICMOS observations, and summarize the properties of the sample. We also estimate the contamination rates and the selection volume for this sample. Finally, we use this search to derive a constraint on the volume density of $L^*_{z=3}$ (or $\sim$−21 mag) galaxies at $z \sim 7$. We will also incorporate results from the $\sim$248 arcmin^2 (Bouwens et al. 2008) search for $z \sim 7$ galaxies in deep ground-based data over GOODS.

The structure of this paper is as follows. In Section 2, we summarize the observational data. In Section 3, we describe our search results for $z \gtrsim 7$ galaxies. In Section 4, we use the observational search results to derive a constraint on the bright end of the $z \sim 7$ and $z \sim 9$ UV LFs. Finally, we provide a summary (Section 5). Throughout this work, we often denote luminosities in terms of the characteristic luminosity $L^*_{z=3}$ at $z \sim 3$ (Steidel et al. 1999), i.e., $M_{\rm UV,AB} = -21.07$ (though this LF determination has recently been updated: Reddy & Steidal 2009). Where necessary, we assume $\Omega_0 = 0.3$, $\Omega_\Lambda = 0.7$, $H_0 = 70$ km s^{-1} Mpc^{-1}. Although these parameters are slightly different from those determined from the *Wilkinson Microwave Anisotropy Probe* seven-year results (Komatsu et al. 2010),

Table 1
ACS + NICMOS + Ground-based Imaging Data used for our z and J Dropout Searches[a]

Name	Area	5σ Depth[b]				Ref
		z_{850}	J_{110}	H_{160}	K_s	
New NICMOS fields						
GOODS NICMOS Survey	44.6	27.5	...[c]	26.9	~25[g]	(1)
Teplitz Parallels[d]	9.3	27.5	...[c]	26.9	~25[g]	(2)
HDF-S	4.3	26.4	26.3[e]	26.7	25.7	(3)
Yan Survey	3.1[f]	27.5	26.9	26.7	...	(4)
Henry Fields	3.4[f]	27.5	26.9	26.7	...	(5)
NICMOS fields already considered by Bouwens et al. (2008)						
HDF-N Dickinson	4.0	27.8	27.0	27.0	25.6	(6,7)
HDF-N Thompson	0.8	27.8	28.0	28.1	25.6	(8,7)
HUDF Thompson	5.8	29.0	27.6	27.4	26.0	(9,10)
HUDF Stiavelli	0.7	29.0	28.1	27.9	26.0	(10,11)
HUDF-NICPAR1	1.3	28.6	28.6	28.4	...	(11,12)
HUDF-NICPAR2	1.3	28.6	28.6	28.4	...	(11,12)
GOODS Parallels	9.3	27.5	27.0	26.9	~25[g]	(12)
Fields with ground-based data already considered in Bouwens et al. (2008)						
ISAAC v2.0 (CDF-S)	136	27.5	~25.4[g]	~24.8[g]	~25[g]	(13)
MOIRCS GTO-2 (HDF-N)	28	27.5	25.6	...	25.6	(7)
MOIRCS GTO-1,3,4 (HDF-N)	84	27.5	24.2	...	24.4	(7)

Notes.
[a] The layout of these search fields is illustrated in Figure 1.
[b] 5σ depths for ACS and NICMOS data given for a 0.″6 diameter aperture and for a ~1.″0 diameter aperture for the ground-based K_s-band data. No correction has been made for the nominal light outside these apertures (for example, for a point source, the correction is typically ~0.2 mag) to keep the present estimates as empirical as possible. This is in contrast to the convention that we use in some previous work (e.g., Bouwens et al. 2008) where such corrections have been made.
[c] NICMOS J_{110}-band observations with 5σ depths of 27.0 mag (0.″6 diameter aperture) were acquired in those fields with $z \gtrsim 7$ candidates.
[d] 40-orbit NICMOS H_{160}-band observations taken in parallel with ACS SBC far-UV observations of the HUDF (Siana et al. 2007; GO10403: PI: Teplitz)
[e] The J-band observations here are from the deep FIRES observations over the HDF-S with ISAAC (Labbé et al. 2003).
[f] Not including the overlap with the GOODS NICMOS Survey (Conselice et al. 2010).
[g] The depth of the near-IR data over the CDF-S varies by ~0.2–0.4 mag depending upon the observational conditions in which the ISAAC data were taken (Mannucci et al. 2007; Stanway et al. 2008; Retzlaff et al. 2010).
References. (1) Conselice et al. 2010, (2) Siana et al. (2007), (3) Labbé et al. (2003), Zirm et al.(2007) (4) H. Yan et al. (2010, in preparation) (5) Henry et al.(2009), (6) Dickinson 1998, (7) Kajisawa et al. 2006, Ouchi et al. 2007, (8) Thompson et al. 1999, (9) Thompson et al. (2005), (10) Labbé et al. (2006), (11) Oesch et al. 2007, (12) Bouwens & Illingworth (2006), Riess et al. (2007), Siana et al. (2007), (13) Retzlaff et al. 2010, Mannucci et al. 2007, Stanway et al.(2008).

they allow for convenient comparison with other recent results expressed in a similar manner. We express all magnitudes in the AB system (Oke & Gunn 1983).

2. OBSERVATIONAL DATA

The present search for galaxy candidates at $z \gtrsim 7$ makes use of ~88 arcmin^2 of deep NICMOS + ACS observations over the two GOODS fields + HDF-S, as well as ~248 arcmin^2 of deep MOIRCS + ISAAC ground-based data.

Table 1 provides a convenient summary of the observational properties of each of these search fields, while Figure 1 shows their position within the two GOODS fields. A significant part of these observations (e.g., those over the HDF-N, Williams et al. 1996; HUDF, Beckwith et al. 2006; NICMOS parallels to HUDF) have already been used to search for $z \gtrsim 7$ galaxies (e.g., Bouwens et al. 2008; Oesch et al. 2009), and so we will not repeat a detailed description of those observations here.

Instead we focus on the NICMOS observations taken over the past three years not yet utilized for $z \gtrsim 7$ searches. These observations include 317 orbits of NICMOS data from five different *HST* programs (GO9723, GO10403, GO11082, GO11144, and GO11192) over $\gtrsim$60 arcmin^2.

The foundation of our search for new $z \gtrsim 7$ candidates is provided by the NICMOS observations of the first three programs (GO9723, GO10403, and GO11082). These programs involve 236 orbits of H_{160}-band NICMOS imaging observations, and cover ~58 arcmin^2 of the ~65 arcmin^2 of new search area.[10] One hundred and eighty of these orbits came from the GOODS NICMOS Survey (Conselice et al. 2010: GO11082), with 60 separate three-orbit NIC3 pointings. Forty of the orbits were obtained in parallel with ACS SBC far-UV observations over the HUDF (Siana et al. 2007; GO10403: PI: Teplitz), and 16 of the orbits came from a NICMOS program over the HDF-S WFPC2

[10] We note that a small fraction (~3–4 arcmin^2) of this search area had been previously considered (Henry et al. 2009).

field (Labbé et al. 2003; GO9723: PI: Franx), with 8 two-orbit NIC3 pointings. We have indicated the positions of those NIC3 pointings that lie within the GOODS fields on Figure 1 with light orange squares. These observations were reduced with our NICMOS pipeline "nicred.py" (Magee et al. 2007) and reach 26.7 and 26.9 mag (5σ, 0.″6 diameter apertures) depending upon whether the H_{160}-band integrations were two or three orbits, respectively, in duration. The FWHM for the H_{160}-band point-spread function (PSF) is ∼0.″37.

The first two of these programs (GO10403 and GO11082) had deep optical coverage from the GOODS ACS program, with corresponding depths reaching 27.9, 28.1, 27.4, and 27.3 in the B_{435}, V_{606}, i_{775}, and z_{850} bands, respectively, in 0.″6 diameter apertures. Our reductions of the ACS GOODS observations are described in Bouwens et al. (2007) and take advantage of essentially all Advanced Camera for Surveys (ACS) data ever taken over the GOODS fields. They are similar to the GOODS v2.0 reductions, but reach ∼0.1–0.3 mag deeper in the z_{850} band due to the inclusion of the supernovae (SNe) follow-up data (Riess et al. 2007). The third program here (GO9723) had deep WFPC2 observations from the HDF-S program (Williams et al. 2000), and 2-orbit i_{775}/2-orbit z_{850} ACS WFC observations as part of the ACS GTO program (PI: Ford; GTO 9301).

The IRAC reductions we use for our selection of $z \gtrsim 7$ galaxy candidates are those from Dickinson & GOODS Team (2004). They reach to 27.4 mag, 26.8 mag, 25.4 mag, and 25.3 mag in the 3.6 μm, 4.5 μm, 5.8 μm, and 8.0 μm bands, respectively, at 1σ (2″) in most regions (where 23 hr integrations are considered) and 0.4 mag deeper (where the integration time is 46 hr).

Deep J_{110}-band observations became available over some fraction of these fields as a result of our 60-orbit GO11144 NICMOS program. The J_{110}-band observations were ∼2–3 orbits in duration, reaching depths of 26.9–27.0 mag (5σ in 0.″6 diameter aperture) and targeted specific $z \gtrsim 7$ candidates identified in the original ACS optical + NICMOS H_{160}-band observations (see Section 3.2 for a description of the preselection). Only 14 such NIC3 fields were obtained and are indicated in Figure 1 with the magenta squares (though two of the NIC3 fields shown targeted specific $z \sim 6$ candidates to allow for a measurement of the UV-continuum slope β: see Bouwens et al. 2009b). Again the reduction of those observations was performed with "nicred.py" (Magee et al. 2007), an alignment made to the ACS GOODS data, and then the data drizzled onto the ACS GOODS frame rebinned on a 0.″09 × 0.″09 frame. The FWHM for the J_{110}-band PSF is ∼0.″33.

Two of our NIC3 fields chosen for J_{110}-band follow-up were allocated more than three orbits of time to better ascertain the nature of the $z \gtrsim 7$ candidates in those fields. In the first case (S4: 03:32:42.48, −27:42:48.8), additional follow-up observations were obtained with NICMOS. In the other case (S2: 03:32:06.75, −27:47:07.0), additional follow-up observations were obtained with WFC3/IR in the J_{125} band (one orbit).

While most of the search power of our program is provided by the first three H_{160}-band programs and the follow-up J_{110}-band program, we also include observations from two other *HST* programs in our search for $z \gtrsim 7$ galaxies. One of these programs is the H. Yan et al. (2010, in preparation) GO 11192 program designed to follow up on bright z_{850}-dropout candidates identified in wide-area ground-based near-IR observations over the two GOODS fields (see the dark orange squares in Figure 1 annotated with "Y"). In that program, 4-orbit (J_{110} + H_{160})-band observations (two orbits in the J_{110} band and two orbits in the H_{160} band) were obtained on six different bright $z \sim 7$ candidates. These fields reached depths of 26.9 and 26.7 mag in the J_{110} and H_{160} bands, respectively, in 0.″6 diameter apertures.

The other program that we utilized was GO10872 (Henry et al. 2009; Siana et al. 2010). NICMOS parallel observations from that program cover ∼3.4 arcmin^2 of area and lie within the two GOODS fields (see the dark orange squares in Figure 1 annotated with "H"). These observations reach to ∼26.9 mag in the J_{110} band and ∼26.7 mag in the H_{160} band. While Henry et al. (2009) have already used these fields to search for candidate $z \gtrsim 7$ galaxies—reporting none—we shall nevertheless incorporate these observations into our $z \gtrsim 7$ search to be as comprehensive as possible.

3. SELECTION OF $z \gtrsim 7$ CANDIDATES

Here we describe the selection of $z \gtrsim 7$ galaxies over those NICMOS fields not previously considered by our team for such searches (∼65 arcmin^2 in search area). We will not revisit the searches for $z \gtrsim 7$ galaxies conducted by Bouwens et al. (2008) over the ∼23 arcmin^2 of area within the HUDF, HDF-N, and CDF-S or the ∼248 arcmin^2 of deep ground-based data. Instead we will simply incorporate the Bouwens et al. (2008) search results in with our new search results.

3.1. Catalogs

We use the same procedure for performing object detection and photometry as we have used in previous work (e.g., Bouwens et al. 2007; Bouwens et al. 2008). Briefly, we begin by PSF-matching all of our data to the PSF of our detection image (which here is the NICMOS H_{160} band). SExtractor (Bertin & Arnouts 1996) is then run in double-image mode, with detection image taken to be the square root of the χ^2 image (Szalay et al. 1999). Here the square root of the χ^2 image is simply the NICMOS H_{160}-band imaging data. Colors were measured in a smaller scalable aperture using Kron (1980) photometry, with a Kron factor of 1.2 to improve the S/N (typical aperture diameters for color measurements were 0.″4). To correct the small-aperture flux measurements to total magnitudes, we computed corrections by comparing the light in a larger scalable (Kron factor of 2.5) aperture on the χ^2 image with that in the smaller aperture (Kron factor of 1.2). Figure 5 of Coe et al. (2006) provides a graphical description of a similar multi-stage procedure for measuring colors and total magnitudes. We also make a small correction for light outside the larger scalable apertures and on the wings of the PSF (typically ∼0.15 mag). This correction is made based upon the encircled energy expected to lie outside this aperture (for stars).

3.2. $z \gtrsim 7$ Candidate Preselection

Searches for star-forming galaxies at high redshift tend to be relatively straightforward in execution. Typically, these searches involve the acquisition of imaging data in three adjacent bands followed by a traditional two-color Lyman break galaxy (LBG) selection. While useful, this approach is limited by the available resources. Often times, much larger areas can be searched by utilizing suboptimal data sets that still allow for the efficient identification of high-redshift star-forming galaxies.

With the availability of deep wide-area NICMOS H_{160}-band data over the two GOODS + HDF-S fields, we have such a data set. The wide-area NICMOS + optical + IRAC data allow us to identify sources that have a high probability of corresponding to $z \gtrsim 7$ galaxies. We can perform such a preselection due to the

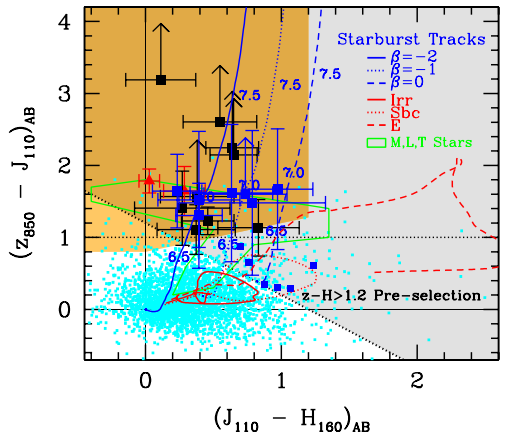

Figure 2. $z_{850} - J_{110}$ vs. $J_{110} - H_{160}$ color–color diagram used to select $z \sim 7$ z_{850}-dropouts. The orange region shows the location of $z \sim 7$ candidates in color–color space. The expected colors of high-redshift star-forming galaxies and low-redshift galaxy contaminants (shown over the redshift range $z \sim 0$–2) are indicated with the blue and red lines, as a function of redshift. The plotted uncertainties and limits are 1σ (consistent with previous work). The green line encloses the region in color–color space where we expect low-mass stars to be found (e.g., Knapp et al. 2004), while the red triangles show the positions of two probable T dwarfs identified within the GOODS fields (Bouwens et al. 2008; Mannucci et al. 2007). The cyan points show the colors of individual sources in our search fields. The light-shaded gray region shows the $z_{850} - H_{160} > 1.2$ preselection we use to identify possible $z \gtrsim 7$ candidates to follow up with deeper J_{110}-band NICMOS observations (Section 3.2). It is apparent that this preselection identifies all eight $z \sim 7$ candidates (large black squares) previously found by Bouwens et al. (2008) and the Bradley et al. (2008) $z \sim 7.6$ galaxy. The large blue squares show the colors of sources that satisfied our $z \sim 7$ z_{850}-dropout criteria and are included in our $z \sim 7$ z_{850}-dropout sample (Tables 2 and 4), while the small blue squares show the colors of preselected galaxies that did not (and hence are more likely at low redshift). See Table 2 for our photometry on those $z \gtrsim 7$ candidates identified for J_{110}-band follow-up observations.

(A color version of this figure is available in the online journal.)

unique colors of star-forming galaxies at $z \gtrsim 7$. $z \gtrsim 7$ galaxies are very red in the optical to H_{160} colors and moderately blue in the H_{160} to IRAC colors.

We then follow up these preselected candidates with deep imaging in the J_{110} band to better ascertain their nature using more traditional two-color LBG criteria. For $z \sim 7$ galaxies (Section 3.3), we apply the same $z_{850} - J_{110}/J_{110} - H_{160}$ criterion utilized by Bouwens et al. (2004b), Bouwens & Illingworth (2006), and Bouwens et al. (2008). Candidates with very red $z_{850} - J_{110}$ colors (corresponding to the Lyα cutoff) and blue $J_{110} - H_{160}$ colors (corresponding to the UV continuum) are taken to be $z \sim 7$ galaxies.

For the $z \gtrsim 7$ preselection, we employ Lyman-break-like criteria. The candidates must be detected at $\geqslant 5\sigma$ in the H_{160} band, have $(z_{850} - H_{160})_{AB}$ colors redder than 1.2, be completely undetected ($<2\sigma$) in the ACS B_{435}, V_{606}, and i_{775} bands, and not have $H_{160} - 5.8\,\mu$m colors redder than 2.5 mag (to exclude dust-reddened galaxies at $z \sim 1$–2). Our use of a $z_{850} - H_{160} > 1.2$ preselection was designed to ensure that the candidates we identified showed a prominent break across the z_{850} and H_{160} bands (as expected for $z \gtrsim 7$ dropouts). However, this criterion was not so strong as to exclude any $z \sim 7$ z_{850}-dropout galaxies identified in previous NICMOS searches (e.g., Bouwens et al. 2008; Oesch et al. 2009) or to have a substantial impact on the effective selection volume of our $z \gtrsim 7$ search.

Sources that were detected at 1.5σ in more than two optical bands (B_{435}, V_{606}, or i_{775}) were also excluded. Figure 2 illustrates this preselection in terms of the $z_{850} - J_{110}/J_{110} - H_{160}$ standard two-color diagram used to identify $z \sim 7$ z_{850}-dropout galaxies.

We identified 20 $z \gtrsim 7$ candidates for follow-up study from the wide-area ($\sim$58 arcmin^2) NICMOS H_{160}-band observations. The coordinates and photometry for candidates are listed in Table 2. After some experimentation, we discovered that we could fit those $z \gtrsim 7$ candidates within 14 $52'' \times 52''$ NIC3 fields (i.e., S1, S2, S3, S4, S5, S6, S7, S8, N1, N3, N4, N5, N6, N7).

We obtained follow-up J_{110}-band NICMOS observations on these candidates (typically three orbits for each NIC3 pointing) with the 60-orbit *HST* GO program 11144. Those observations were obtained from 2007 December 19 to 2008 September 9, with one final orbit of observations taken on 2009 October 26 with the WFC3/IR camera. The positions of these follow-up data are illustrated in Figure 1 with the magenta squares (and rectangle for the 1-orbit WFC3/IR observation).

Once the NICMOS J_{110}-band observations were obtained, we redid our photometry on each $z \gtrsim 7$ candidate. This photometry is included in Table 2 for all 20 $z \gtrsim 7$ candidates identified for follow-up study. We then applied the z_{850}- and J_{110}-dropout selection criteria we describe in the next two subsections to identify probable star-forming galaxies at $z \sim 7$ and $z \sim 9$, respectively, from this preselection.

3.3. $z \sim 7$ z_{850}-dropout Selection

We use the same selection criterion for identifying $z \sim 7$ z_{850}-dropouts as we did in our previous work on the HUDF and two GOODS fields (Bouwens et al. 2008). Specifically, we require our z_{850}-dropout candidates to satisfy the criteria $((z_{850} - J_{110})_{AB} > 0.8) \wedge ((z_{850} - J_{110})_{AB} > 0.8 + 0.4(J_{110} - H_{160})_{AB})$, where $\wedge$ represents the logical **AND** symbol. In cases of a non-detection in the dropout band, the flux in the dropout band is set to its 1σ upper limit. This two-color selection is illustrated in Figure 2 with the positions of the $z \gtrsim 7$ candidates from Table 2 included as the large blue squares.

z_{850}-dropout candidates are required to be detected at 5σ in the H_{160} band (0.″6 diameter aperture) to ensure that they correspond to real sources. In addition, included in the present search are also those sources from the NICMOS observations from the H. Yan et al. (2010, in preparation) GO 11192 and Henry et al. (2009) GO 10872 programs.

In total, seven sources from our new search fields satisfied our z_{850}-dropout criteria. All of these candidates were found over the GOODS NICMOS Survey fields (Conselice et al. 2010), and none from the H. Yan et al. (2010, in preparation) or Henry et al. (2009) fields. Postage stamps of these candidates are shown in Figure 3. Flux measurements for the candidates are given in Table 6 in Appendix A. The sources range in magnitude from $H_{160,AB} \sim 25.4$ to 26.2 mag, with most of the sources being found at $\sim$26 mag. The surface density of z_{850}-dropout candidates in our fields ($\sim$65 arcmin^2) brightward of 26.5 mag is $\sim$0.1 source arcmin^{-2}, very similar to that found by Bouwens et al. (2008).

Overall, the properties ($J_{110} - H_{160}$ color and sizes) of most of our candidates seem consistent with their being high-redshift galaxies. The mean half-light radius (including the effect of the PSF) is $\sim$0.″25, which is similar to the candidates found over the HUDF (e.g., Bouwens et al. 2008). Meanwhile, the $J_{110} - H_{160}$ color for the sources is 0.6 ± 0.1 mag. This is consistent with, albeit somewhat higher than, the $J_{110} - H_{160} \sim 0.48$ color expected from our simulations (Bouwens et al. 2008), assuming a $\beta \sim -2$ (Bouwens et al. 2010a; Stanway et al. 2005; Finkelstein et al. 2010; Bunker et al. 2010). Nonetheless, a few of the candidates (GNS-zD3 and GNS-zD5) in our selection

Table 2
$z \gtrsim 7$ Candidates in Our Wide-area NICMOS H_{160}-Band Data Preselected for J_{110}-Band Follow-up Observations[a]

ID	R.A.	Decl.	NICMOS Follow-up Pointing[b]	$B-H$	$V-H$	$i-H$	$z-H$	$z-J$	$J-H$	H	$\sigma(H)$[c]
				$z \sim 7$ z_{850}-dropout candidates							
GNS-zD1[d]	03:32:43.29	−27:42:47.9	S4	>3.2	>3.7	2.7 ± 0.7	1.7 ± 0.3	1.3 ± 0.4	0.4 ± 0.2	25.8 ± 0.2	9
GNS-zD2	03:32:32.03	−27:45:37.2	S5	>2.6	2.9 ± 0.6	>2.3	>2.2	1.6 ± 1.0	0.6 ± 0.3	26.2 ± 0.3	5
GNS-zD3[e,f]	03:32:06.10	−27:46:37.3	S2	>3.1	>3.4	>2.9	>2.5	1.5 ± 1.0	0.8 ± 0.5	26.1 ± 0.3	5
GNS-zD4	12:36:10.93	62:09:15.6	N3	>2.6	>3.0	>2.4	>2.3	>1.6	0.7 ± 0.3	25.8 ± 0.3	6
GNS-zD5[f]	12:36:44.68	62:16:15.4	N4	>3.3	>3.6	>3.2	>2.5	1.7 ± 0.8	1.0 ± 0.3	25.4 ± 0.2	10
GNS-zD6[d,g]	03:32:22.66	−27:43:00.6	S1	>3.2	>3.4	>2.6	1.9 ± 0.4	1.6 ± 0.5	0.2 ± 0.2	25.4 ± 0.2	11
GNS-zD7[d,h]	03:32:42.84	−27:42:47.7	S4	>2.5	>3.0	>2.3	1.9 ± 0.5	1.5 ± 1.0	0.4 ± 0.3	26.1 ± 0.2	5
				$z \sim 9$ J-dropout candidates							
GNS-JD1[i]	03:32:13.77	−27:52:42.8	S8	...	2.9 ± 0.9	2.5 ± 0.9	>1.9	>0.5	1.4 ± 0.5	25.7 ± 0.2	6
GNS-JD2[j]	12:36:25.47	62:14:31.8	N2	>3.3	>3.4	>2.5	>2.3	...	>2.0	25.8 ± 0.3	6
				Probable spurious J-dropout candidates[k]							
GNS-Sp1	03:33:04.66	−27:52:27.0	S3	...	>3.4	>3.2	2.3 ± 0.5	...	>2	26.5 ± 0.3	5
GNS-Sp2	03:33:04.14	−27:52:57.4	S3	...	>3.4	>3.0	>2.3	...	>2	26.0 ± 0.2	5
GNS-Sp3	03:32:08.06	−27:46:58.1	S2	>2.9	>3.1	>2.9	>2.4	...	>2.1	27.0 ± 0.3	5
				Other candidates targeted in preselection[l]							
GNS-O1	03:33:02.18	−27:53:40.4	S6	>2.0	>2.2	0.8 ± 0.6	1.7 ± 0.8	0.9 ± 0.8	0.7 ± 0.5	26.7 ± 0.3	5
GNS-O2	03:32:27.81	−27:54:48.0	S7	2.7 ± 0.6	>3.4	>2.9	1.4 ± 0.4	0.3 ± 0.5	1.1 ± 0.4	25.1 ± 0.2	7
GNS-O3	12:36:15.21	62:10:39.7	N6	>2.3	>2.5	>2.0	1.4 ± 0.5	0.6 ± 0.7	0.8 ± 0.6	26.7 ± 0.3	5
GNS-O4	12:36:11.26	62:09:00.0	N3	2.1 ± 0.6	>2.8	>2.2	1.3 ± 0.5	0.3 ± 0.6	0.9 ± 0.5	26.3 ± 0.3	5
GNS-O5	12:36:19.14	62:15:23.4	N1	2.8 ± 0.9	>3.0	>2.6	1.8 ± 0.6	0.6 ± 0.7	1.2 ± 0.4	25.5 ± 0.2	5
GNS-O6	12:36:31.68	62:06:45.8	N5	>2.7	2.6 ± 0.6	>2.4	>2.3	...	>2.0	26.2 ± 0.3	5
GNS-O7	12:37:06.51	62:11:49.0	N7	>2.8	>3.0	>2.6	2.1 ± 0.6	<−0.2	>1.9	26.1 ± 0.3	5
GNS-O8	12:37:03.01	62:11:35.8	N7	>3.0	>3.1	>2.7	1.2 ± 0.3	0.3 ± 0.4	0.9 ± 0.3	26.0 ± 0.3	6

Notes.

[a] Lower limits are 1σ.

[b] NIC3 pointing (from GO11144) used for J_{110}-band follow-up observations on specific $z \gtrsim 7$ candidates. Fourteen different NIC3 pointings were utilized (S1, S2, S3, S4, S5, S6, S7, S8, N1, N3, N4, N5, N6, and N7).

[c] Significance (in σ) of the H_{160}-band detection. The significance is measured in our smaller scalable apertures (Kron factor of 1.2). These apertures are smaller than those used for estimates of the total magnitudes (Section 3.1), and hence the associated significance levels are accordingly higher.

[d] Flux information is also available on these candidates from the WFC3/IR ERS program (see Table 3).

[e] WFC3/IR J_{125}-band data are also available for GNS-zD3 as a result of our GO 11144 program. The measured J_{125}-band magnitude for this candidate is 26.5 ± 0.2 mag. The $J_{125} - H_{160}$ color (0.4 ± 0.3) is somewhat red for a $z \sim 7$ galaxy. GNS-zD3 is thus more likely at low redshift than most candidates in our selection.

[f] These $z \sim 7$ candidates are sufficiently red in their $J_{110} - H_{160}$ colors that there is an increased probability they could be low-redshift contaminants. We have no evidence for this possibility however.

[g] Also identified in Castellano et al. (2010) and Hickey et al. (2010).

[h] This source has a measured $z_{850} - Y_{105}$ color $\sim 0.0 \pm 1.0$ and $J_{125} - H_{160} \sim 0.6 \pm 0.2$ color in the high S/N WFC3/IR observations (see Table 3). This suggests this candidate may be a red $z \sim 1$–2 galaxy and not a $z \sim 7$ star-forming galaxy.

[i] GNS-JD1 is detected at 1σ in the V_{606} and i_{775} bands, not sufficient to rule it out as a $z \sim 9$ J_{110}-dropout candidate, but suggesting that it may lie at $z \sim 1$–2.

[j] We have no evidence that GNS-JD2 is detected at wavelengths other than 1.6 μm (H band). It is sufficiently close to another source that it is unclear if it is detected redward of 2 μm from the IRAC data. This may suggest that it is a transient source (SNe: see Section 3.4) or spurious (since it is close to the edge of the NIC3 field where it was found). However, we cannot rule out the possibility that it corresponds to a $z \sim 9$ galaxy (but we consider it unlikely).

[k] These candidates were targeted for follow-up observations based upon $\sim 5\sigma$ detections in the NICMOS H_{160}-band data. However, they are not detected in the NICMOS J_{110}-band observations. Lacking such detections, their reality is less secure. We suspect that they may be spurious (see Section 3.4).

[l] These candidates were targeted for J_{110}-band follow-up observations with NICMOS (because of their red $z_{850} - H_{160} > 1.2$ colors, apparent absence of flux in the optical, and moderately blue $H - 5.8$ μm colors: see Section 3.1). However, they do not satisfy our $z \sim 7$ z_{850}- or $z \sim 9$ J_{110}-dropout criteria.

have sufficiently red $J_{110} - H_{160}$ colors ($\sim$0.8–1.0 mag) that they might be low-redshift interlopers.

The NICMOS J_{110}-band observations available on GNS-zD3 were only moderately deep ($\sim$2 orbits) and so GNS-zD3 only shows a weak detection in that band. Fortunately, we were able to obtain deeper J_{125}-band observations on GNS-zD3 with the WFC3/IR instrument (Section 2). The new data confirm that there is a detection in the J band, and the measured magnitude 26.5 ± 0.2 is consistent with what is found with NICMOS.

Three of our new z_{850}-dropout candidates (GNS-zD1, GNS-zD6, and GNS-zD7) are found over the upper region in the CDF-S where deep wide-area WFC3/IR observations were recently taken as part of the Early Release Science program (GO11359: PI: O'Connell). Given that these observations reach $\sim$0.7-1.0 mag deeper than the NICMOS observations utilized in this study and extend over three bands, Y_{098}, J_{125}, and H_{160}, they are useful for characterizing the typical dropout candidates found in this search.

What do these deeper data suggest about the candidates in our selection? Photometry on the three aforementioned z_{850}-dropout candidates was performed using the new WFC3/IR observations (utilizing specifically the Bouwens et al. 2010c reductions). The results are summarized in Table 3, and the conclusions are mixed. GNS-zD6 is clearly a $z \sim 6$ galaxy—though from the measured colors its redshift is likely in the range $z \sim 6.2$–6.5. The nature of GNS-zD1 is slightly less clear from the data. Its measured $z - J$, $Y - J$ colors are consistent with it being

Table 3
Available WFC3/IR Photometry for $z \sim 7$ z_{850}-Dropout Galaxy Candidates in our Wide-area NICMOS Sample

Object ID	R.A.	Decl.	H_{160}	NICMOS		WFC3/IR		
				$z_{850} - J_{110}$	$J_{110} - H_{160}$	$z_{850} - Y_{098}$	$Y_{098} - J_{125}$	$J_{125} - H_{160}$
GNS-zD1	03:32:43.29	−27:42:47.9	25.8 ± 0.2	1.3 ± 0.4	0.4 ± 0.2	0.8 ± 0.4	0.6 ± 0.3	0.2 ± 0.1
GNS-zD6	03:32:22.66	−27:43:00.6	25.4 ± 0.2	1.6 ± 0.5	0.2 ± 0.2	1.4 ± 0.4	0.0 ± 0.2	0.4 ± 0.1
GNS-zD7[a]	03:32:42.84	−27:42:47.7	26.1 ± 0.3	1.5 ± 1.0	0.4 ± 0.3	0.5 ± 0.9	0.5 ± 0.6	0.7 ± 0.3

Note.[a] The measured $z_{850} - Y_{105}$ color ∼0.0 ± 1.0 and $J_{125} - H_{160}$ color $\sim 0.6 \pm 0.2$ suggest that this candidate may be a red $z \sim$ 1–2 galaxy and not a $z \sim 7$ star-forming galaxy.

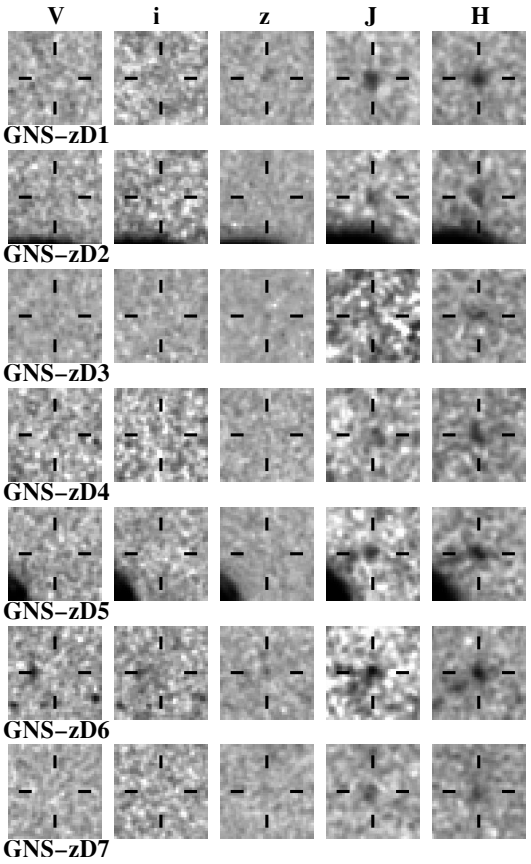

Figure 3. $V_{606} i_{775} z_{850} J_{110} H_{160}$ images (3.″5 × 3.″5) of the seven $z \sim 7$ z_{850}-dropout candidates identified in our new wide-area NICMOS data. See Table 2 for the coordinates, magnitudes, colors, and other properties of the present z_{850}-dropout candidates. Deeper J_{125}-band observations with the WFC3/IR camera were obtained over GNS-zD3 to confirm the weak J_{110}-band detection obtained with NICMOS. The nature of GNS-zD7 is unclear. While the source satisfies our z_{850}-dropout criterion (and would therefore appear to be a plausible $z \sim 7$ galaxy), its $Y - J$, $J - H$ colors measured with WFC3/IR suggest a red $z \sim$ 1–2 galaxy.

either a $z \sim 6.5$ galaxy or a red $z \sim$ 1–2 galaxy. The blue $J - H \sim 0.1$ colors of GNS-zD1 seem to slightly favor the case that it is a $z \gtrsim 5$ galaxy. Finally, GNS-zD7 seems most consistent with being an intrinsically red $z \sim$ 1–2 galaxy, having very red $J - H \sim 0.6$, $Y - J \sim 0.7$ colors.

These results suggest that the present z_{850}-dropout selection is successful in identifying $z \gtrsim 6.5$ galaxies, albeit with a mean redshift somewhat lower than the $z \sim 7.3$ estimated in Bouwens et al. (2008). The lower mean redshift for the sample is consistent with the expected bias based upon evolution across the z_{850}-dropout selection window (where more luminous galaxies are present, e.g., at $z \sim 6.5$ than at $z \sim 8$: Muñoz & Loeb 2008). The likely contamination of our selection by one

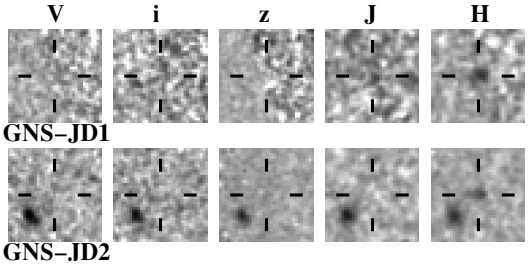

Figure 4. $V_{606} i_{775} z_{850} J_{110} H_{160}$ images (3.″5 × 3.″5) of the two sources in our new wide-area NICMOS data that satisfy our $z \sim 9$ J_{110}-dropout criteria. However, we consider it unlikely that either of the candidates identified here corresponds to a $z \sim 9$ galaxy. GNS-JD1 appears to be detected at 1σ in both the V_{606} and i_{775} bands, not sufficient for us to rule it out as a $z \sim 9$ J_{110}-dropout candidate but suggesting that it may be a $z \sim$ 1–2 galaxy. GNS-JD2, by contrast, shows no evidence for being detected at wavelengths other than 1.6 μm (H band). This may suggest that it is a transient source (SNe: see Section 3.4) or spurious (since it is close to the edge of the NIC3 field where it was found). However, we cannot rule out the possibility that it corresponds to a $z \sim 9$ galaxy (but we consider it very unlikely). See Tables 2 and 6 for the coordinates, magnitudes, colors, and other properties of these candidates.

probable low-redshift source (GNS-zD7) is consistent with the 24% contamination rates estimated in Section 3.6.

The principal reason we are finding modest levels of contamination over the GOODS fields is because of the limited depth of the available ACS optical data over the GOODS fields. This contamination is somewhat higher than estimated over other $z \sim 7$ z_{850}-dropout selections like the HUDF—where it was estimated to be ∼12% (e.g., Bouwens et al. 2008). In order to reduce these contamination levels, it would therefore be ideal if deeper optical data—particularly in the F606W, F775W, and F814W bands—could be obtained over the GOODS fields.

3.4. $z \sim 9$ J_{110}-dropout Selection

Similar to our $z \sim 7$ z_{850}-dropout selection, we adopt the same $z \sim 9$ J_{110}-dropout selection criteria as we used in the ∼23 arcmin^2 Bouwens et al. (2008) NICMOS search. J_{110}-dropout candidates in our selection are required to satisfy the criterion $(J_{110} - H_{160})_{AB} > 1.3$ and not show $> 2\sigma$ detections in any of the optical bands (or $> 1.5\sigma$ in two bands). $z \sim 9$ J_{110}-dropout candidates are also required to be detected at 6σ in the H_{160} band (0.″6 diameter aperture) to ensure that most of the sources are real. We use a 6σ detection criterion for our J_{110}-dropout selection (instead of a 5σ criterion) because we only have one passband to evaluate the reality of the candidates.

In total, we identified two sources that satisfied our $z \sim 9$ J_{110}-dropout criteria. Postage stamps of these candidates are provided in Figure 4, and their photometry is summarized in Table 2. Flux measurements for the candidates are given in Table 6 in Appendix A.

While both candidates formally satisfy our J_{110}-dropout selection criteria and therefore may correspond to $z \sim 9$ galaxies, neither candidate is very compelling and there are reasons to suspect that each candidate may be a contaminant. For example, GNS-JD1 is formally detected at 1σ in both the V_{606} and i_{775} bands—suggesting that it may actually correspond to a $z \sim 2$ Balmer-break galaxy. In addition, GNS-JD1 is detected at 5σ in both the $3.6\,\mu$m and $4.5\,\mu$m bands, with $m_{3.6\,\mu\mathrm{m}} = 25.1 \pm 0.2$ mag and $m_{4.5\,\mu\mathrm{m}} = 25.0 \pm 0.2$ mag. This latter IRAC photometry was performed by modeling the light profiles of nearby neighbors in the IRAC imaging data, subtracting these model profiles from the observations, and then measuring the flux in simple 2.″5 diameter apertures (e.g., Labbé et al. 2006; González et al. 2010; Labbé et al. 2010a).

The other J_{110}-dropout candidate GNS-JD2 is also quite possibly spurious. None of the observations at other wavelengths provide any evidence it is real. It is not detected in the ACS observations, the NICMOS J_{110}-band observations, nor even the IRAC 3.6μm and 4.5μm observations. The non-detection of the candidate is particularly noteworthy at $3.6\,\mu$m, and it would represent a very significant concern if it were not so close to a neighboring source. However, because of this, the flux measurements are sufficiently challenging that the IRAC non-detection does not definitely argue against the reality of the source. Nonetheless, the non-detection does suggest that the original detection of GNS-JD2 in the H_{160} band may have been anomalous and therefore the source is likely either spurious or a transient source (i.e., a SN).

Additional evidence for the source being spurious comes from its proximity to the edge of the NIC3 field where it was found (due to enhanced non-Gaussianity of the noise there). To test the spurious hypothesis, we examined the individual NICMOS exposures that went into its H_{160}-band stack. None of these exposures provided a dominant contribution to the cumulative H_{160}-band flux, leaving us with no compelling reason to flag this particular candidate as spurious. An alternative hypothesis is that GNS-JD2 is a SN. As we discuss in Section 3.6, we would expect $\sim$1 SN to be identified over our $\sim$58 arcmin^2 H_{160}-band observations as a $z \gtrsim 7$ galaxy candidate.

Besides these two formal J_{110}-dropout candidates, there were three other $z \gtrsim 7$ candidates identified in the NICMOS H_{160}-band data for follow-up (GNS-Sp1, GNS-Sp2, and GNS-Sp3 in Table 2), but which were not detected in the later J_{110}-band observations. This would give these sources nominal $J_{110} - H_{160}$ colors $\gtrsim$2 mag (1σ) and make them possible $z \sim 9$ J_{110}-dropout candidates. However, there are reasons to be concerned about these candidates and whether they correspond to real sources. While the formal significance of each source is $\sim 5\sigma$ in the H_{160}-band data, these sources are detected in stacks of $\leqslant$9 NICMOS exposures (and hence subject to noise with significant non-Gaussian signatures) and are typically near a bright source (GNS-Sp1 and GNS-Sp3). Consequently, the true significance of these sources is somewhat smaller, i.e., $\lesssim 4\sigma$, making it more likely that they are spurious (see also the simulation results in Section 3.6).[11] These three sources are included in Table 2 under the label "Probable spurious J-dropout candidates."

[11] Note that this is in contrast to situations where similar significance sources are found in observations created from a much larger number of exposures (e.g., the 56-exposure stacks used for the WFC3/IR HUDF09 H_{160}-band observations: Oesch et al. 2010a; Bouwens et al. 2010b). In those cases, the noise characteristics are much closer to Gaussian, and apparent 5σ sources are indeed significant at the 5σ level.

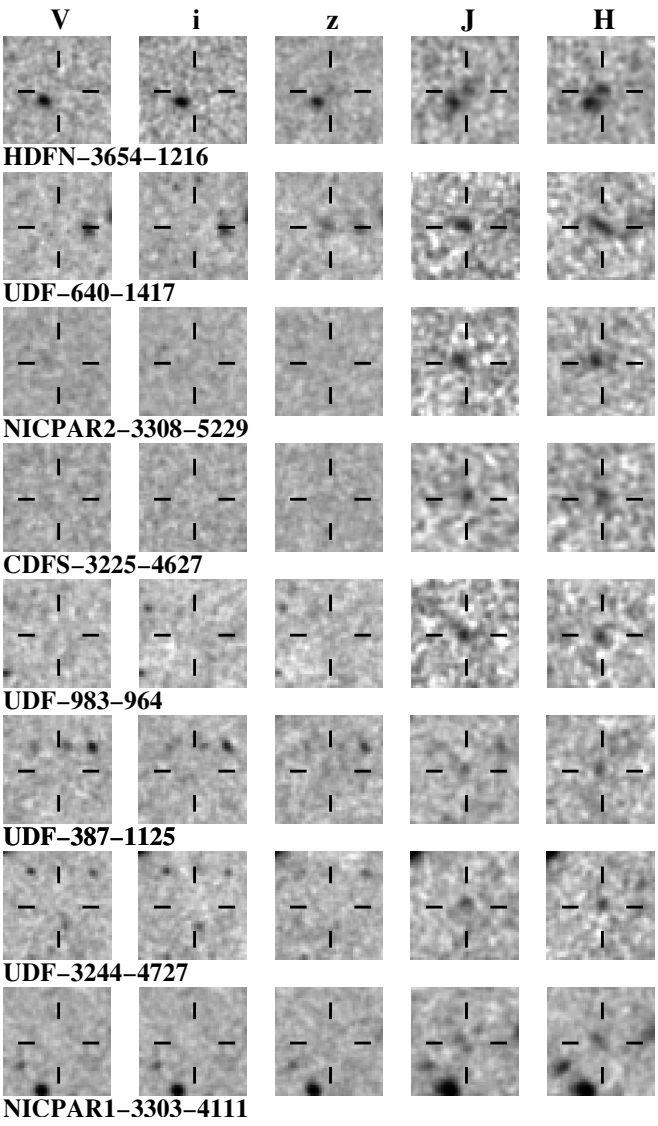

Figure 5. $V_{606}i_{775}z_{850}J_{110}H_{160}$ images of the 8 $z \sim 7$ z_{850}-dropout candidates previously identified in the ultra-deep, wide-area NICMOS data (Bouwens et al. 2008; but see also e.g., Oesch et al. 2009), but now utilizing the deeper J_{110}-band observations (eight additional orbits) obtained on two candidates (UDF-3244-4727 and UDF-387-1125) as part of the GO 11144 program. The J_{110}-band detections for these two candidates are now much more significant than they were in Bouwens et al. (2008; Figure 3 from that work). The other six candidates are included here for completeness. Each of the above candidates is detected at $\geqslant 4.5\sigma$ in both the J_{110} and H_{160} bands.

3.5. Total Sample of $z \sim 7$ z_{850} and $z \sim 9$ J_{110} Dropouts

In Sections 3.3 and 3.4, we identify seven plausible $z \sim 7$ z_{850}-dropout candidates in the deep, wide-area ($\sim$65 arcmin^2) NICMOS H_{160}-band data recently obtained over the GOODS + HDF-S fields. Two possible $z \sim 9$ J_{110}-dropout candidates are identified, but appear unlikely to correspond to $z \sim 9$ galaxies. To increase our search area to $\sim$88 arcmin^2 (including all the NICMOS observations in Table 1), we combine this sample with the sample of $z \gtrsim 7$ dropouts found in the deep, but smaller area $\sim$23 arcmin^2 NICMOS data already considered by Bouwens et al. (2008). Figure 5 shows postage stamp images of the $z \sim 7$ field candidates from that study. Those postage stamps are essentially identical to those presented in Bouwens et al. (2008), but incorporate eight additional orbits of NICMOS observations taken on two HUDF z_{850}-dropout candidates (UDF-387-1127,

Table 4
A Complete Sample of $z \sim 7$ z_{850}-Dropout Galaxy Candidates Selected from NICMOS Observations Over the CDF-S + HDF-N GOODS Fields, the HUDF, and Galaxy Cluster Fields (see Table 1)[a]

Object ID	R.A.	Decl.	H_{160}	$z_{850} - J_{110}$	$J_{110} - H_{160}$	$H_{160} - K_s$	$M_{UV,AB}$[b]	Ref
Candidates in the CDF-S and HDF-N fields								
GNS-zD5	12:36:44.68	62:16:15.4	25.4 ± 0.2	1.7 ± 0.8	1.0 ± 0.3	...	−21.5	...
GNS-zD6	03:32:22.66	−27:43:00.6	25.4 ± 0.2	1.6 ± 0.5	0.2 ± 0.2	...	−21.5	(12,13)
GNS-zD4	12:36:10.93	62:09:15.6	25.8 ± 0.3	>1.6	0.7 ± 0.3	...	−21.1	...
GNS-zD1	03:32:43.29	−27:42:47.9	25.8 ± 0.2	1.3 ± 0.4	0.4 ± 0.2	...	−21.1	...
HDF-N-3654-1216	12:36:54.12	62:12:16.2	26.0 ± 0.1	1.1 ± 0.3	0.4 ± 0.3	0.0 ± 0.3	−20.9	(2,7)
GNS-zD3	03:32:06.10	−27:46:37.3	26.1 ± 0.3	1.5 ± 1.0	0.8 ± 0.5	...	−20.8	...
GNS-zD7[c]	03:32:42.84	−27:42:47.7	26.1 ± 0.2	1.5 ± 1.0	0.4 ± 0.5	...	−20.8	...
UDF-640-1417	03:32:42.56	−27:46:56.6	26.2 ± 0.1	1.3 ± 0.3	0.5 ± 0.2	0.5 ± 0.3	−20.7	(1,2,3,4,5,7,11,12)
GNS-zD2	03:32:32.03	−27:45:37.2	26.2 ± 0.3	1.6 ± 1.0	0.6 ± 0.3	...	−20.7	...
NICPAR2-3308-5229[d]	03:33:08.29	−27:52:29.2	26.7 ± 0.1	> 2.2[e]	0.6 ± 0.2	...	−20.2	(7,8)
CDFS-3225-4627	03:32:25.22	−27:46:26.7	26.7 ± 0.2	1.4 ± 0.5	0.2 ± 0.3	<0.2[e]	−20.2	(2,7)
UDF-983-964	03:32:38.80	−27:47:07.2	26.9 ± 0.2	>3.2[e]	0.1 ± 0.3	0.0 ± 0.8	−20.0	(1,2,4,5,7,8,11)
UDF-387-1125[f]	03:32:42.56	−27:47:31.4	27.1 ± 0.2	1.3 ± 0.5	0.8 ± 0.4	<0.0[e]	−19.8	(1,5,7,11)
UDF-3244-4727[f]	03:32:44.02	−27:47:27.3	27.3 ± 0.2	>2.6[e]	0.5 ± 0.4	<0.1[e]	−19.6	(7,8)
NICPAR1-3303-4111[d]	03:33:03.81	−27:41:12.1	27.8 ± 0.1	>1.5[e]	0.4 ± 0.2	...	−19.1	...
Candidates in lensing cluster fields[a]								
A1689-zD1	13:11:29.73	−01:19:20.9	24.7 ± 0.1	>2.2[e]	0.6 ± 0.2	...	−19.8	(6)
CL0024-zD1	00:26:37.93	17:10:39.0	25.6 ± 0.1	1.3 ± 0.8	0.4 ± 0.3	...	−19.3	(9)
CL0024-iD1	00:26:37.78	17:10:40.0	25.0 ± 0.1	0.9 ± 0.2	0.1 ± 0.1	...	−19.9	(9)

Notes.
[a] There are a few weaker z_{850}-dropout candidates behind lensing clusters that have been identified by Richard et al. (2008) and Bouwens et al. (2009a), but none of these has deep enough optical data to be included in the present list as a reliable $z \sim 7$ candidate.
[b] The absolute magnitudes estimated for the sources are for an effective rest-frame wavelength of ∼1900 Å. The absolute magnitudes given for the lensed sources include a correction for the estimated magnification factor (Bradley et al. 2008; Zheng et al. 2009).
[c] This source has a measured $z_{850} - Y_{105}$ color ∼0.0 ± 1.0 and $J_{125} - H_{160}$ color ∼ 0.6 ± 0.2 in the high S/N WFC3/IR observations (see Table 3). This suggests this candidate may be a red $z \sim 1$–2 galaxy and not a $z \sim 7$ star-forming galaxy.
[d] See the footnotes in Table 2 of Bouwens et al.(2008) for these candidates.
[e] Upper and lower limits on the measured colors are the 1σ limits.
[f] The S/N on our J_{110}-band fluxes for UDF-387-1127 and UDF-3244-4727 is higher than initially reported in Bouwens et al. (2008). The improved S/N is the result of eight orbits of additional J_{110}-band observations on these sources.
References. (1) Bouwens et al. (2004b), (2) Bouwens & Illingworth (2006), (3) Yan & Windhorst (2004), (4) Coe et al. (2006), (5) Labbé et al. (2006), (6) Bradley et al. (2008), (7) Bouwens et al. (2008), (8) Oesch et al. (2009), (9) Zheng et al. (2009), (10) González et al. (2010), (11) Oesch et al. (2010a), McLure et al. (2010), Bunker et al. (2010), Yan et al. (2010), Finkelstein et al. (2010), (12) Castellano et al. (2010), (13) Hickey et al. (2010).

UDF-3244-4727) in the J_{110} band.

Our total sample of $z \sim 7$ z_{850}-dropouts identified in our search fields (Table 1)—including both the old and new data—is presented in Table 4. Also included in this table are three $z \sim 7$ z_{850} dropouts identified in searches behind lensing clusters (Bradley et al. 2008; Bouwens et al. 2009; Zheng et al. 2009).

3.6. Estimated Contamination Rate

High-redshift dropout selections are subject to contamination from (1) sources that enter the selection due to photometric scatter, (2) transient sources, (3) low-mass stars, and (4) spurious sources (i.e., corresponding to no real source). We consider each of these sources of contamination in examining the present $z \sim 7$ z_{850}- and $z \sim 9$ J_{110}-dropout selections.

Possible contamination from photometric scatter. In general, the most important contaminant for high-redshift dropout selections are sources that enter the selections due to photometric scatter (e.g., see Bouwens et al. 2008, 2010b). We estimate the contamination rate that results from this effect by starting with the color distribution observed for $H \sim 25.0$–26.5 sources in the HUDF09 WFC3/IR field (Bouwens et al. 2010b; Oesch et al. 2010a) and then adding photometric scatter to match that expected for each source in our NICMOS catalogs. Repeating these simulations for each source in our NICMOS catalogs (from all search fields not considered in Bouwens et al. 2008), we predict that 1.7 and 0.2 sources would enter our z_{850}- and J_{110}-dropout selections, respectively, via photometric scatter. The implied contamination rates are 24% and 10%, respectively, which are somewhat higher than estimates for our HUDF z_{850}-dropout selections (Bouwens et al. 2008) or for our new WFC3/IR results (Oesch et al. 2010a; Bouwens et al. 2010b). This is due to the somewhat shallower depths of the ACS optical data over the GOODS fields and larger prevalence of low-redshift sources with similar colors to high-redshift galaxies at bright magnitudes (see also Section 3.3). The above procedure is essentially identical to that used in Bouwens et al. (2008).

Possible contamination from transient sources. Contamination from transient sources, particularly SNe, is potentially important for each of our search fields, given that the NICMOS observations were typically acquired at least four years after the ACS optical observations. Using the GOODS SNe searches (Riess et al. 2004; Strolger et al. 2004) as a baseline, Bouwens et al. (2008) argued that the contamination rate from SNe should be no larger than 0.012 arcmin^{-2} for observations where the optical and near-IR J+H observations are taken at very different times. This suggests a contamination rate of ∼1 source for the present search for $z \gtrsim 7$ galaxies over ∼65 arcmin^2 of new data. However, the above calculation assumes that the J- and H-band observations are acquired at the same time. In reality, for most of the new data, the J_{110}-band observations were taken at least 3–12 months after the NICMOS H_{160}-band observations for each of our new z_{850}-dropout candidates. Consequently, the

measured $J-H$ colors for SNe found in the GOODS NICMOS survey would likely be very red and hence show up as an apparent J_{110}-dropout candidate. We might therefore expect one SN contaminant to be present in our J_{110}-dropout selection. This may be the case for GNS-JD2 (see Section 3.4).

Possible contamination from low-mass stars. Low-mass stars (e.g., T or L dwarfs) have very similar $z-J$, $J-H$ colors to star-forming galaxies at $z\sim 7$ and therefore could contaminate our z_{850}-dropout selection. Given the modest resolution of the NICMOS data, it is difficult to use these data to clearly distinguish small ($\sim$0.″15 half-light radius) star-forming galaxies found at $z\sim 7$ from unresolved low-mass stars. Fortunately, the z_{850}-band observations have sufficient resolution and depth that low-mass stars (with $z-J$ colors $\sim$1.5–2) would be evident at 5σ (0.″2 diameter aperture) in the z_{850}-band images as point sources. Only one possible T dwarf candidate is evident in the new wide-area NICMOS observations and that is the source at 03:32:22.66 and −27:43:00.6 (GNS-zD6). However, that source appears to be resolved in the new WFC3/IR observations as part of the Early Release Science Program (GO11359: PI: O'Connell), so that source appears unlikely to be a low-mass star. The present situation is somewhat in contrast to the NICMOS observations considered by Bouwens et al. (2008) where two probable T dwarfs were identified in selecting $z\gtrsim 7$ galaxies (included on Figure 2 as the red triangles).

Possible contamination from spurious sources. Contamination from spurious sources could be a concern for our $z\sim 9$ J_{110}-dropout selection. Each of our J_{110}-dropout candidates is only detected in a single band and the estimated $\sim 6\sigma$ significance of these detections may be an overestimate (due to real data possessing many non-Gaussian characteristics). Therefore, to estimate the likely number of spurious sources, we used the standard negative image test (e.g., Dickinson et al. 2004) and repeated our $z\sim 9$ J_{110}-dropout selection on the negative H_{160}-band images (after masking out sources brighter than 23 mag). Such a selection yielded $\sim$12 J_{125}-dropout candidates, but all of the candidates (on the negative images) could be eliminated due to an obvious association with defects or irregularities in the reduction. While this might suggest that spurious sources do not dominate our J_{110}-dropout selection, there were a modest number of formal 5σ detections on the negative images quite close to satisfying our J_{110}-dropout selection criteria, and so contamination from spurious sources here is certainly not impossible.

By contrast, for our $z\sim 7$ z_{850}-dropout selection, spurious sources are not an important concern. Each of our candidates is detected at $\gtrsim 2\sigma$ in the J_{110} band and $\gtrsim 5\sigma$ in the H_{160} band—making contamination from spurious sources extremely unlikely.

Summary. In total, we expect 1.7 and 1.2 contaminants in our $z\sim 7$ z_{850}- and $z\sim 9$ J_{110}-dropout selections, respectively (equivalent to contamination levels of 24% and 60%). The only meaningful source of contamination for our z_{850}-dropout selections is photometric scatter, while for our J_{110}-dropout selection, several sources of contamination contribute. We expect $\sim$1 contaminant from transient sources (SNe), 0.2 contaminants from photometric scatter, and $\lesssim$1 contaminant from spurious sources.

4. IMPLIED CONSTRAINTS ON THE REST-FRAME UV LUMINOSITY FUNCTION

The present wide-area ($\sim$88 arcmin^2) NICMOS search for $z\gtrsim 7$ candidates provides a useful constraint on the volume density of luminous star-forming galaxies at $z\sim 7$ and $z\sim 9$. These observations cover twice as much area as $\sim$39 arcmin^2 ERS observations and cover a similar area to that available from the CDF-South HAWK-I observations (90 arcmin^2: Castellano et al. 2010; Hickey et al. 2010). They therefore provide a somewhat comparable constraint on the bright end (i.e., $M_{UV}<-20.7$) of the $z\gtrsim 7$ LFs to these studies. And while the Ouchi et al. (2009) Subaru Suprime-Cam search extends over considerably more area (1568 arcmin^2) than these observations, the present NICMOS search is somewhat deeper than that study (by $\sim$0.7 mag). The present search also benefits from somewhat higher quality multiwavelength data—deep high-resolution ACS or mid-IR IRAC data (Giavalisco et al. 2004; Dickinson & GOODS Team 2004)—than are generally available for the Subaru fields. This allows for a more robust discrimination between high-redshift star-forming galaxies and low-redshift contaminants (and low-mass stars).

Here we will estimate the stepwise LF $\Phi(M)$ using the relatively simple $V/V_{\rm eff}$ approach (e.g., Steidel et al. 1999) where

$$\Phi(m)=\frac{N(m)}{V_{\rm eff}(m)}, \quad (1)$$

where $N(m)$ is the number of $z\gtrsim 7$ candidates in a given magnitude interval m (from all of our search fields) and $V_{\rm eff}(m)$ is the effective volume in the magnitude interval m.

To compute the effective volume with which we can select star-forming galaxies in our various search fields, as a function of magnitude and redshift, we run detailed Monte Carlo simulations where we introduce model galaxies into the observed data and attempt to select them as dropouts using the procedures laid out in Section 3. These simulations are performed in the same way as they were performed in Bouwens et al. (2008). For the model galaxies in these simulations, we assume that the $z\gtrsim 7$ galaxies of a given luminosity have similar pixel-by-pixel morphologies to $z\sim 4$ galaxies in the HUDF with the same luminosity, but scaled in size as $(1+z)^{-1}$ to match the observed size–redshift trends at $z\geqslant 2$ (e.g., Ferguson et al. 2004; Bouwens et al. 2004a; Bouwens et al. 2006; Oesch et al. 2010b). The UV-continuum slopes of the model galaxies are assumed to have a mean of -2, with a 1σ scatter of 0.5. These latter assumptions match the colors of bright star-forming galaxies found at $z\sim 7$ (Bouwens et al. 2008, Bouwens et al. 2010b; Oesch et al. 2010a; Bunker et al. 2010; Finkelstein et al. 2010).

In computing UV LFs on the basis of our $z\gtrsim 7$ search, we consider all seven $z\sim 7$ z_{850}-dropout candidates in the newest NICMOS data and suppose that $\sim$5.3 z_{850}-dropout candidates from this search correspond to $z\sim 7$ galaxies (accounting for the 24% contamination rate estimated in Section 3.6). We also incorporate the constraints from the NICMOS + ground-based $z\sim 7$ search considered by Bouwens et al. (2008). In addition, we suppose that $\lesssim$1 J_{110}-dropout candidates from this search correspond to $z\sim 9$ galaxies, given the concerns that exist for each candidate (Section 3.4). Finally, the $z\sim 7$ and $z\sim 9$ LFs are only redetermined here at luminosities where we can take advantage of the new $\sim$65 arcmin^2 of NICMOS observations (see Table 1).

Our stepwise UV LF at $z\sim 7$ is presented in Table 5 and in Figure 6 (left). For comparison, Figure 6 also includes the $z\sim 7$ LFs of Bouwens et al.(2008), Oesch et al. (2009), Ouchi et al. (2009), Castellano et al.(2010), Oesch et al. (2010a), McLure et al. (2010), and Bouwens et al. (2010c). The present LF results are in reasonable agreement with previous determinations. In the right panel of Figure 6, the present $z\sim 7$ LF results are shown relative to the LFs at $z\sim 4$, $z\sim 5$, $z\sim 6$ (from Bouwens

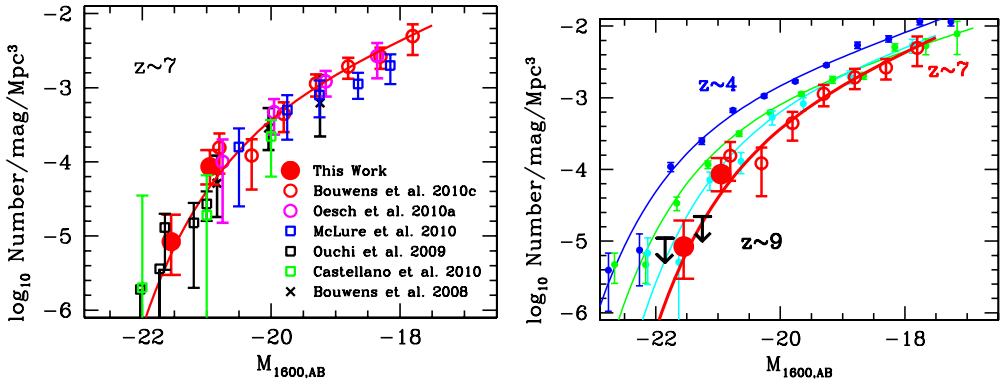

Figure 6. Left: present determination of the stepwise UV LF at $z \sim 7$ using deep wide-area NICMOS + ground-based observations (large solid red circles: see Section 4). The $z \sim 7$ UV LF is only redetermined here at luminosities where we can take advantage of the new ~65 arcmin^2 of NICMOS observations (see Table 1) to search for candidate $z \gtrsim 7$ galaxies. For comparison, we also show the $z \sim 7$ LFs reported by Bouwens et al. (2008: black crosses), Ouchi et al. (2009: black squares), Castellano et al. (2010: green squares), Oesch et al. (2010a: open magenta circles), McLure et al. (2010: blue squares), and Bouwens et al.(2010c: open red circles). Constraints from Wilkins et al. (2010b) are similar, but not shown to reduce confusion. The solid red line is the best-fit Schechter function presented in Oesch et al. (2010a). Right: stepwise UV LF determined here at $z \sim 7$ (solid red circles) vs. that derived at $z \sim 4$ (blue), $z \sim 5$ (green), and $z \sim 6$ (cyan) by Bouwens et al. (2007). The open red circles and red line represent the $z \sim 7$ LF determined by Bouwens et al.(2010c). Also shown are our constraints on the LF at $z \sim 9$ from the present J_{110}-dropout search (black upper limits: see Section 4). Similar to the situation for our $z \sim 7$ LF, the $z \sim 9$ J_{110}-dropout LF is only computed at luminosities where we can take advantage of the new NICMOS data. The volume densities of $\sim L^*_{z=3}$ (~ -21 mag) star-forming galaxies at $z \sim 7$ and $z \sim 9$ are 13^{+8}_{-5} times and >25 times lower, respectively, than at $z \sim 4$.

(A color version of this figure is available in the online journal.)

Table 5
Stepwise Constraints on the Rest-frame UV LF at $z \sim 7$ and $z \sim 9$ from Wide-area NICMOS + Ground-based Observations (Section 4)[a]

$M_{\rm UV,AB}$[b]	ϕ_k (10^{-6} Mpc^{-3} mag^{-1})
z_{850}-dropouts ($z \sim 7$)	
−21.55	8^{+11}_{-5}
−20.95	86^{+58}_{-37}
J-dropouts ($z \sim 9$)	
−21.85	< 11[c]
−21.25	< 22[c]

Notes.
[a] The UV LFs are only redetermined here at luminosities where we can take advantage of the new ~65 arcmin^2 of NICMOS observations (see Table 1) to search for candidate $z \gtrsim 7$ galaxies.
[b] The effective rest-frame wavelength is ~1900 Å for our z_{850}-dropout selection and ~1500 Å for our J_{110}-dropout selection.
[c] Upper limits here are 1σ (68% confidence).

et al. 2007) to provide a sense of the evolution from $z \sim 4$. Also included on this figure (black upper limits) are the constraints on the UV LF at $z \sim 9$ from the present J_{110}-dropout search. The UV LF is 13^{+8}_{-5} times lower at $z \sim 7$ than at $z \sim 4$ and >25 times lower (1σ) at $z \sim 9$ than at $z \sim 4$. The latter constraint is the most stringent constraint yet available on the volume density of $\gtrsim L^*_{z=3}$ galaxies at $z \sim 9$.

Of course, the above LF determinations are subject to uncertainties as a result of large-scale structure (cosmic variance) and therefore, to properly frame the above results, it is helpful to estimate the size of these uncertainties. For convenience, we utilize the Trenti & Stiavelli (2008) cosmic variance calculator to make this estimate. Given that the approximate volume densities of the sources probed at $z \sim 7$ and $z \sim 9$ are $\sim 8 \times 10^{-5}$ Mpc^{-3} and $\sim 2 \times 10^{-5}$ Mpc^{-3}, respectively, the approximate bias parameters are 10 and 12, respectively (e.g., Somerville et al. 2004; Trenti & Stiavelli 2008). Given that our NICMOS search data are fairly randomly scattered over the two GOODS fields, we assume two independent search fields of dimension $10' \times 16'$ and adopt a width for our redshift selection window $\Delta z \sim 1.5$ (e.g., see Figure 7 of Bouwens et al. 2008). Utilizing these inputs, we estimate that the large-scale structure uncertainties on our LF results here are ~17% and ~20%, respectively. Large-scale structure uncertainties are therefore much smaller than those uncertainties estimated from the small number statistics (~8 sources) and uncertain contamination rates (Section 3.6).

5. SUMMARY

We have taken advantage of ~88 arcmin^2 of deep, wide-area NICMOS data to search for $z \gtrsim 7$ galaxies within the HUDF, the two GOODS fields, and the HDF-S. This search incorporates ~65 arcmin^2 of wide-area NICMOS data not previously used to identify $z \gtrsim 7$ galaxies.[12] We also consider ~248 arcmin^2 of deep ground-based data ($\gtrsim$25.5 mag, 5σ) previously used by Bouwens et al. (2008). In total, we find ~7 plausible $z \sim 7$ z_{850}-dropout candidates in the new NICMOS observations (six of which are being reported for the first time) and ~2 possible (but probably unlikely) $z \sim 9$ J_{110}-dropout candidates. These candidates significantly add to the number of luminous $z \gtrsim 7$ candidates known within the GOODS fields and improve our constraints on the volume density of luminous galaxies at $z \sim 7$. These candidates have recently been used to model the stellar populations of bright $z \sim 7$ galaxies (González et al. 2010; Labbé et al. 2010b).

When taken together with the NICMOS data already considered in Bouwens et al. (2008), we have identified 15 $z \sim 7$ z_{850}-dropout candidates in total from ~88 arcmin^2 of deep NICMOS data. After running detailed simulations to estimate the selection volumes and contamination rates, we use our new $z \sim 7$ samples (plus ground-based search area) to update the Bouwens et al. (2008) determination of the UV LF at $z \sim 7$ and to strengthen our constraints on the LF at $z \sim 9$.

We find that the bright end of the UV LF at $z \sim 7$ is 13^{+8}_{-5} times lower at $z \sim 7$ than at $z \sim 4$. At $z \sim 9$, the UV LF is a factor of >25 times lower (1σ) than at $z \sim 4$, assuming that

[12] A small fraction of these 65 arcmin^2 (4 arcmin^2) had previously been used by Henry et al. (2009) for a $z \sim 7$ z_{850}-dropout search.

Table 6
Measurements of the Fluxes of Our $z \gtrsim 7$ Candidates in the Optical ACS and Near-IR NICMOS Data[a]

Object ID	f_ν (nJy)					
	B_{435}	V_{606}	i_{775}	z_{850}	J_{110}	H_{160}
GNS-zD1	-10 ± 9	0 ± 6	15 ± 12	35 ± 14	124 ± 13	169 ± 21
GNS-zD2	0 ± 9	9 ± 7	-8 ± 13	12 ± 13	69 ± 14	116 ± 21
GNS-zD3	-2 ± 8	6 ± 6	-5 ± 9	12 ± 13	64 ± 29	130 ± 25
GNS-zD4	5 ± 17	9 ± 13	-14 ± 22	-9 ± 23	102 ± 24	201 ± 32
GNS-zD5	-2 ± 13	-1 ± 9	-29 ± 14	23 ± 17	105 ± 22	258 ± 28
GNS-zD6	3 ± 14	-8 ± 10	33 ± 17	46 ± 21	208 ± 29	258 ± 25
GNS-zD7	9 ± 13	-15 ± 9	-3 ± 16	21 ± 18	93 ± 17	128 ± 26
GNS-JD1	...	7 ± 8	20 ± 16	-29 ± 26	53 ± 17	140 ± 22
GNS-JD2	1 ± 8	3 ± 7	9 ± 8	16 ± 9	-20 ± 16	166 ± 26

Note. [a] Uncertainties here are 1σ. $m_{AB} = 31.4 - 2.5 \log_{10}(f_\nu[\mathrm{nJy}])$.

at most one of the J_{110}-dropout candidates identified here is at $z \sim 9$.

We are grateful to our *HST* program coordinator Beth Perrillo and contact scientist Luigi Bedin for the substantial assistance they provided in setting up the follow-up observations (GO11144) for all of the $z \gtrsim 7$ candidates we identified in deep NICMOS H_{160}-band data. We are thankful to Louis Bergeron, Susan Kassin, and Rodger Thompson for their help in reducing the NICMOS data used in this study. This work also benefited from stimulating conversations with Romeel Davé, Claude-André Faucher-Giguère, Kristian Finlator, Cedric Lacey, Pascal Oesch, Masami Ouchi, and Piero Rosati. The comments of the anonymous referee significantly improved the clarity of the paper. We appreciate Pascal Oesch's careful reading of this paper. We acknowledge support from NASA grants HST-GO09803.05-A, HST-GO10937.03-A, HST-GO11082.04-A, HST-GO11144.03-A, and NAG5-7697.

APPENDIX

FLUX MEASUREMENTS FOR OUR INDIVIDUAL $z \gtrsim 7$ CANDIDATES

To better assess the significance of the colors measured for our $z \gtrsim 7$ candidates, we also tabulate the observed fluxes of each candidate in Table 6. The tabulated fluxes also allow us to readily evaluate whether any of the candidates is detected in the optical (and therefore not likely at high redshift).

REFERENCES

Beckwith, S. V. W., et al. 2006, AJ, 132, 1729
Bertin, E., & Arnouts, S. 1996, A&AS, 117, 39
Bouwens, R. J., & Illingworth, G. D. 2006, Nature, 443, 189
Bouwens, R. J., Illingworth, G. D., Blakeslee, J. P., Broadhurst, T. J., & Franx, M. 2004a, ApJ, 611, L1
Bouwens, R. J., Illingworth, G. D., Blakeslee, J. P., & Franx, M. 2006, ApJ, 653, 53
Bouwens, R. J., Illingworth, G. D., Franx, M., & Ford, H. 2007, ApJ, 670, 928
Bouwens, R. J., Illingworth, G. D., Franx, M., & Ford, H. 2008, ApJ, 686, 230
Bouwens, R. J., et al. 2004b, ApJ, 616, L79
Bouwens, R. J., et al. 2009a, ApJ, 690, 1764
Bouwens, R. J., et al. 2009b, ApJ, 705, 936
Bouwens, R. J., et al. 2010a, ApJ, 708, L69
Bouwens, R. J., et al. 2010b, ApJ, 709, L133
Bouwens, R. J., et al. 2010c, ApJ, submitted (arXiv:1006.4360)
Bradley, L. D., et al. 2008, ApJ, 678, 647
Brandt, W. N., et al. 2001, AJ, 122, 1
Bunker, A., et al. 2010, MNRAS, in press (arXiv:0909.2255)
Castellano, M., et al. 2010, A&A, 511, A20
Coe, D., Benítez, N., Sánchez, S. F., Jee, M., Bouwens, R., & Ford, H. 2006, AJ, 132, 926
Conselice, C. J., et al. 2010, MNRAS, submitted (arXiv:1010.1164)
Dickinson, M. 1998, in The Hubble Deep Field, ed. M. Livio, S. M. Fall, & P. Madau (New York: Cambridge Univ. Press), 219
Dickinson, M., & GOODS Team 2004, BAAS, 36, 1614
Dickinson, M., et al. 2004, ApJ, 600, L99
Ferguson, H. C., et al. 2004, ApJ, 600, L107
Finkelstein, S. L., Papovich, C., Giavalisco, M., Reddy, N. A., Ferguson, H. C., Koekemoer, A. M., & Dickinson, M. 2010, ApJ, 719, 1250
Giavalisco, M., et al. 2004, ApJ, 600, L93
González, V., Labbé, I., Bouwens, R. J., Illingworth, G., Franx, M., Kriek, M., & Brammer, G. B. 2010, ApJ, 713, 115
Henry, A. L., et al. 2009, ApJ, 697, 1128
Hickey, S., Bunker, A., Jarvis, M. J., Chiu, K., & Bonfield, D. 2010, MNRAS, 404, 212
Kajisawa, M., et al. 2006, PASJ, 58, 951
Kimble, R. A., MacKenty, J. W., & O'Connell, R. W. 2006, Proc. SPIE, 6265, 14
Knapp, G. R., et al. 2004, AJ, 127, 3553
Komatsu, E., et al. 2010, ApJS, submitted (arXiv:1001.4538)
Kron, R. G. 1980, ApJS, 43, 305
Labbé, I., Bouwens, R., Illingworth, G. D., & Franx, M. 2006, ApJ, 649, 67
Labbé, I., et al. 2003, AJ, 125, 1107
Labbé, I., et al. 2010a, ApJ, 708, L26
Labbé, I., et al. 2010b, ApJ, 716, L103
Magee, D. K., Bouwens, R. J., & Illingworth, G. D. 2007, in ASP Conf. Ser. 376, Astronomical Data Analysis Software and Systems XVI, ed. R. A. Shaw, F. Hill, & D. J. Bell (San Francisco, CA: ASP), 261
Mannucci, F., Buttery, H., Maiolino, R., Marconi, A., & Pozzetti, L. 2007, A&A, 461, 423
McLure, R. J., Dunlop, J. S., Cirasuolo, M., Koekemoer, A. M., Sabbi, E., Stark, D. P., Targett, T. A., & Ellis, R. S. 2010, MNRAS, 403, 960
Muñoz, J. A., & Loeb, A. 2008, MNRAS, 386, 2323
Oesch, P. A., et al. 2007, ApJ, 671, 1212
Oesch, P. A., et al. 2009, ApJ, 690, 1350
Oesch, P. A., et al. 2010a, ApJ, 709, L16
Oesch, P. A., et al. 2010b, ApJ, 709, L21
Oke, J. B., & Gunn, J. E. 1983, ApJ, 266, 713
Ouchi, M., Tokoku, C., Shimasaku, K., & Ichikawa, T. 2007, in ASP Conf. Ser. 379, Cosmic Frontiers, ed. N. Metcalfe & T. Shanks (San Francisco, CA: ASP), 47
Ouchi, M., et al. 2009, ApJ, 706, 1136
Reddy, N. A., & Steidel, C. C. 2009, ApJ, 692, 778
Retzlaff, J., Rosati, P., Dickinson, M., Vandame, B., Rité, C., Nonino, M., Cesarsky, C., & GOODS Team 2010, A&A, 511, A50
Richard, J., Stark, D. P., Ellis, R. S., George, M. R., Egami, E., Kneib, J.-P., & Smith, G. P. 2008, ApJ, 685, 705
Riess, A. G., et al. 2004, ApJ, 607, 665
Riess, A. G., et al. 2007, ApJ, 659, 98
Rosati, P., et al. 2002, ApJ, 566, 667
Siana, B., et al. 2007, ApJ, 668, 62
Siana, B., et al. 2010, ApJ, 723, 241
Somerville, R. S., Lee, K., Ferguson, H. C., Gardner, J. P., Moustakas, L. A., & Giavalisco, M. 2004, ApJ, 600, L171
Stanway, E. R., Bremer, M. N., Squitieri, V., Douglas, L. S., & Lehnert, M. D. 2008, MNRAS, 386, 370
Stanway, E. R., McMahon, R. G., & Bunker, A. J. 2005, MNRAS, 359, 1184

Steidel, C. C., Adelberger, K. L., Giavalisco, M., Dickinson, M., & Pettini, M. 1999, ApJ, 519, 1
Strolger, L.-G., et al. 2004, ApJ, 613, 200
Szalay, A. S., Connolly, A. J., & Szokoly, G. P. 1999, AJ, 117, 68
Thompson, R. I., Storrie-Lombardi, L. J., Weymann, R. J., Rieke, M. J., Schneider, G., Stobie, E., & Lytle, D. 1999, AJ, 117, 17
Thompson, R. I., et al. 2005, AJ, 130, 1
Trenti, M., & Stiavelli, M. 2008, ApJ, 676, 767
Wilkins, S. M., Bunker, A. J., Ellis, R. S., Stark, D., Stanway, E. R., Chiu, K., Lorenzoni, S., & Jarvis, M. J. 2010a, MNRAS, 403, 938
Wilkins, S. M., Bunker, A. J., Lorenzoni, S., & Caruana, J. 2010b, MNRAS, in press (arXiv:1002.4866)
Williams, R. E., et al. 1996, AJ, 112, 1335
Williams, R. E., et al. 2000, AJ, 120, 2735
Yan, H., & Windhorst, R. A. 2004, ApJ, 612, L93
Yan, H.-J., Windhorst, R. A., Hathi, N. P., Cohen, S. H., Ryan, R. E., O'Connell, R. W., & McCarthy, P. J. 2010, Res. Astron. Astrophys., 10, 867
Zheng, W., et al. 2009, ApJ, 697, 1907
Zirm, A. W., et al. 2007, ApJ, 656, 66